



Reconstruction of late Holocene autumn/winter precipitation variability in SW Romania from a high-resolution speleothem trace element record

Sophie F. Warken^{a,b,*}, Jens Fohlmeister^{c,d}, Andrea Schröder-Ritzrau^b, Silviu Constantin^e, Christoph Spötl^f, Axel Gerdes^g, Jan Esper^h, Norbert Frank^b, Jennifer Arps^b, Mihai Terente^e, Dana F.C. Riechelmann^a, Augusto Mangini^b, Denis Scholz^a

^a Institute of Geosciences, Johannes Gutenberg-University Mainz, Johann-Joachim-Becher-Weg 21, 55128 Mainz, Germany

^b Institute of Environmental Physics, Heidelberg University, Im Neuenheimer Feld 229, 69120 Heidelberg, Germany

^c Institute of Earth and Environmental Science, University of Potsdam, Karl-Liebknecht-Strasse 24, Haus 27, 14476, Germany

^d GFZ German Research Centre for Geosciences, Section 5.2 Climate Dynamics and Landscape Development, Telegrafenberg, 14473 Potsdam, Germany

^e Institute of Speleology "Emil Racovita", Strada Frumosa 31, 010986 Bucuresti, Romania

^f Institute of Geology, University of Innsbruck, Innrain 52, 6020 Innsbruck, Austria

^g Institute of Geosciences, Goethe University Frankfurt, Altenhöferallee 1, 60438 Frankfurt am Main, Germany

^h Department of Geography, Johannes Gutenberg-University Mainz, Johann-Joachim-Becher-Weg 21, 55128 Mainz, Germany

ARTICLE INFO

Article history:

Received 24 April 2017

Received in revised form 12 June 2018

Accepted 19 July 2018

Available online xxxx

Editor: H. Stoll

Keywords:

speleothem

trace elements

proxy calibration

precipitation reconstruction

Romania

North Atlantic forcing

ABSTRACT

We present the first high-resolution trace element (Mg/Ca, Sr/Ca, Ba/Ca) record from a stalagmite in southwestern Romania covering the last 3.6 ka, which provides the potential for quantitative climate reconstruction. Precise age control is based on three independent dating methods, in particular for the last 250 yr, where chemical lamina counting is combined with the identification of the 20th century radiocarbon bomb peak and ²³⁰Th/U dating. Long-term cave monitoring and model simulations of drip water and speleothem elemental variability indicate that precipitation-related processes are the main drivers of speleothem Mg/Ca ratios. Calibration against instrumental climate data shows a significant anti-correlation of speleothem Mg/Ca ratios with autumn/winter (October to March) precipitation ($r = -0.61$, $p < 0.01$), which is statistically robust when considering age uncertainties and auto-correlation. This relationship is used to develop a quantitative reconstruction of autumn/winter precipitation. During the late Holocene, our data suggest a heterogeneous pattern of past regional winter hydroclimate in the Carpathian/Balkan realm, along with intermittent weakening of the dominant influence of North Atlantic forcing. In agreement with other regional paleo-hydrological reconstructions, the observed variability reveals periodically occurring strong NW-SE hydro-climate gradients. We hypothesize, that this pattern is caused by shifts of the eastern edge of the area of influence of the NAO across central-eastern Europe due to the confluence of North Atlantic forcing, and other climatic features such as the East Atlantic/Western Russia (EAWR) pattern.

© 2018 Elsevier B.V. All rights reserved.

1. Introduction

Speleothems have been successfully used for quantitative reconstruction of past climate variability (Cai et al., 2010; Jex et al., 2011; Moquet et al., 2016), e.g., using stable oxygen isotope or annual growth lamina records, considered as reliable recorders of air temperature or precipitation amount (Baker and Bradley, 2010;

Cai et al., 2010; Tan et al., 2013). Proxy records from laminated stalagmites are best suited for calibration with instrumental data, when lamina-counted chronologies are cross-validated with absolute dating methods (Baker et al., 2007; Smith et al., 2009).

Trace element concentrations constitute additional, valuable tracers of past climate variability (Casteel and Banner, 2015; McDonald et al., 2004; Treble et al., 2003). Mg or Sr co-variability is often linked to hydroclimatic processes via water-rock interaction such as prior calcite precipitation (PCP) or drip rate variability (Cruz et al., 2007; McDonald et al., 2004; Sinclair et al., 2012). However, these processes may be confounded by a variety of sec-

* Corresponding author at: Institute of Environmental Physics, Heidelberg University, Im Neuenheimer Feld 229, 69120 Heidelberg, Germany.

E-mail address: sophie.warken@iup.uni-heidelberg.de (S.F. Warken).

ond order effects (Fairchild and Treble, 2009; Smith et al., 2009; Treble et al., 2003). Hence, trace element records have so far only sparsely been used for quantitative reconstruction of past precipitation variability, since establishing a transfer function between a climate parameter at the Earth's surface and the speleothem proxy signals requires a rigorous understanding of the processes involved in the proxy signal transfer from the surface into the cave as well as the in-cave processes (Baker and Bradley, 2010; Casteel and Banner, 2015). More recently, the understanding of the drivers of elemental variability in speleothems has greatly improved by model approaches (Sinclair et al., 2012; Stoll et al., 2012), providing a base for calibration studies with speleothem trace elements.

SW Romania is located in a transition region between central Europe, the Mediterranean and western Eurasia. Regional climate is dominated by the influence of the Carpathian mountain topography and westerly driven circulation patterns (Micu et al., 2015). Over southern and eastern Europe, model studies suggest that positive anomalies of both the North Atlantic Oscillation (NAO) and the East Atlantic/Western Russia pattern (EAWR) are associated with negative precipitation anomalies and vice versa (Bojariu and Paliu, 2001; Ionita, 2014).

Precipitation reconstructions from this region providing information on sub-decadal timescales are mainly based on tree-ring data, which are however limited to the growing season and the past several centuries (Levanič et al., 2012; Popa and Kern, 2008). Longer records, which also give insight in past winter climate conditions, can be provided by cave deposits (Cleary et al., 2017; Constantin et al., 2007; Onac et al., 2002, 2014) and lacustrine or peat-bog records (Feurdean et al., 2015; Longman et al., 2017). Many paleo-hydrological reconstructions suggest that the link of Romanian precipitation to North Atlantic climate variability persisted during the Holocene, e.g., Cleary et al. (2017), Longman et al. (2017) or Onac et al. (2002). However, most studies display strong inter-site variability, which is an indication of the complexity of climate in the Romanian Carpathians and in south-eastern Europe (Longman et al., 2017; Roberts et al., 2012). The incongruities in the understanding of the drivers of past precipitation variability in the Carpathian–Balkan region may partly be a consequence of insufficient accuracy and/or scarcity of the available data (Krichak et al., 2014), since many records are often compromised by a rather coarse temporal resolution.

Here we present a first quantitative autumn/winter precipitation reconstruction from SW Romania based on annually resolved speleothem Mg/Ca record. Combined with a precise age control the calibration is based on a comparison with precipitation data and justified by processes derived from drip site and cave air monitoring. Comprehensive statistical analyses confirm the correlation of speleothem Mg/Ca with instrumental data and enable a transfer function to reconstruct the last 3.6 ka. Hence, this precipitation reconstruction allows inferences on spatial and temporal paleo-hydrological variability in the Southern Carpathian realm on up to (multi-) annual timescales.

2. Material and methods

2.1. Sample description

Cloșani Cave (CC, 45.1°N, 22.8°E) is located at the southern slope of the Carpathians in SW Romania at 433 m above sea level (msl) (Fig. 1A and B). The cave is developed in massive Upper Jurassic limestone mainly consisting of calcite (93%) with minor occurrence of dolomite (7%) (Diaconu, 1990). It consists of two main passages with a total length of 1458 m and a vertical range of 15 m (Fig. 1A, Constantin and Lauritzen, 1999). Stalagmite C09-2 was collected in 2009 beneath the active drip site CC2 (Fig. 2A) in the deeper part of the Crystals passage. At the sampling site, the

host rock overburden is approximately 80–100 m, which is overlain by a up to 1.5 m thick soil, densely covered by vegetation consisting of grasses and shrubs and local tree stands (Constantin and Lauritzen, 1999; Diaconu, 1990). C09-2 has a total length of 70 cm (Fig. 2B). The focus of this study is on the upper 46 cm of C09-2, which are composed of clean, translucent calcite, completely formed by columnar fabric (Fig. S12). This section exhibits both macroscopically (Fig. 2C) and microscopically (Fig. 2D) visible lamination with alternating translucent and whitish lamina.

2.2. Instrumental data

Instrumental data were obtained from the meteorological stations Târgu Jiu (TJ) and Drobeta–Turnu Severin (DTS), located about 50 km east and south-west, respectively, from Cloșani Cave (Fig. 1). TJ provides monthly precipitation sums (P, 1918–2000) and monthly mean temperature (T, 1900–1993), whereas DTS covers P from 1925–2015 and T from 2006–2015 (Klein Tank et al., 2002). Between 1925 and 1999, annual precipitation sums at TJ and DTS correlate with $r_{TJ/DTS,P} = 0.78$ ($r^2 = 0.75$), whereas the relation of autumn/winter (ONDJFM) precipitation is even stronger ($r_{TJ/DTS,PW} = 0.87$, $r^2 = 0.82$). The comparison of seasonal temperature and precipitation patterns indicates that the station data are representative for the cave site (supplemental text S2). In order to assess seasonal infiltration variability, potential evapotranspiration (PET) was estimated applying the equation of Thornthwaite (1948). PET was calculated for the available months from the meteorological stations TJ and DTS. The amount of infiltration P-PET was then estimated by subtracting PET from the measured precipitation amount. The annual cycle of PET and P-PET is illustrated in Fig. 1C. $\delta^{18}O$ values of meteoric precipitation ($\delta^{18}O_p$, data from the Global Network of Isotopes in Precipitation (GNIP), accessible at: <http://www.iaea.org/water>) were obtained from the GNIP station Râmnicu Vâlcea (RV, Fig. 1B) for the years 2012–2015.

2.3. Methods

Drip water (drip interval, pH, $\delta^{18}O$ values as well as concentrations of Ca, Mg, Sr and Ba) and cave air (air temperature, relative humidity, pCO₂) were measured from 2010 to 2015 in bimonthly intervals, while drip interval was additionally monitored using an automatic drip logger from 2010 to 2012 and in 2015.

²³⁰Th/U-dating of speleothem calcite was performed using inductively coupled mass spectrometry (MC-ICPMS) at the University of Heidelberg (Germany). Samples for radiocarbon dating were analyzed at the MICADAS facility in the Klaus-Tschira-Lab (Mannheim, Germany). Stable carbon and oxygen isotope analysis of carbonate was performed using an on-line, automated preparation system linked to a triple collector gas source mass spectrometer at the University of Innsbruck (Austria). Concentrations of trace elements were measured along the major growth axis of C09-2 by laser ablation ICPMS at the University of Frankfurt (Germany). Further details about sample preparation and analytical techniques is given in the supplementary text S1.

The interpretation of trace element variability is supported by the application of I-STAL, a model for interpretation of Mg/Ca, Sr/Ca and Ba/Ca variations in speleothems (Stoll et al., 2012). Correlation analysis was performed with a test statistic based on Pearson's product moment correlation coefficient r and follows a t -distribution with $n - 2$ degrees of freedom. Asymptotic confidence and prediction intervals are given based on Fisher's Z transform and corresponding p -values were adjusted for autocorrelation following Zwiers and von Storch (1995). The correlations of speleothem proxies with instrumental data were calculated with PearsonT3 (Ólafsdóttir and Mudelsee, 2014), which gives confi-

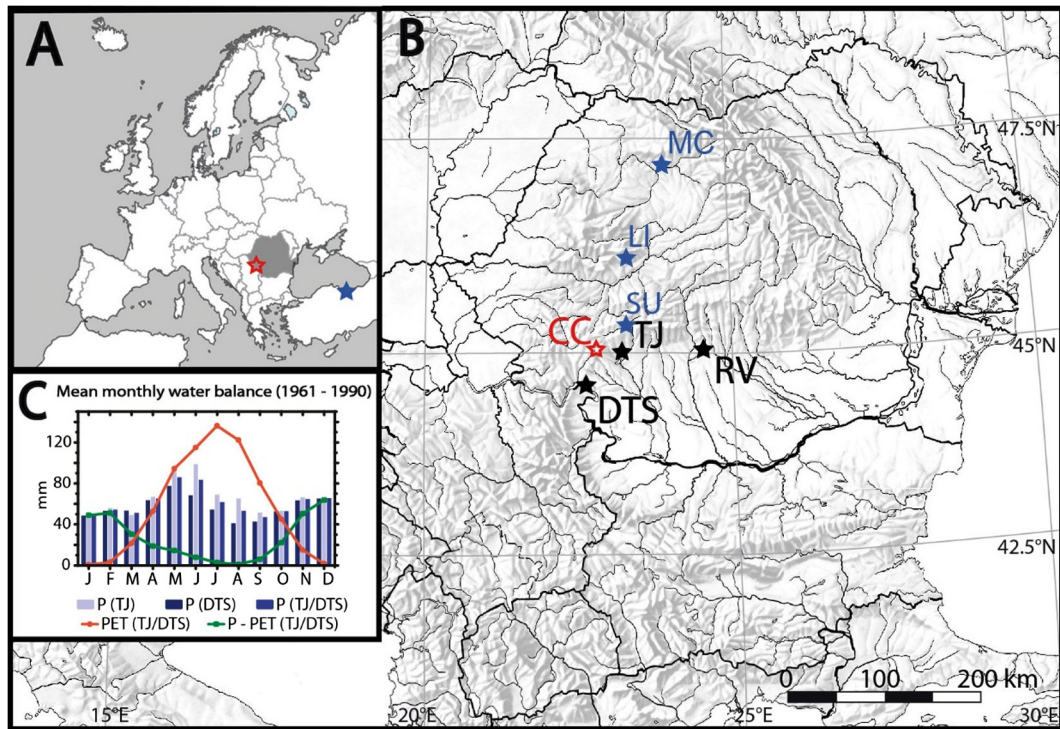


Fig. 1. Locations of the cave site, meteorological stations and important studies mentioned in the text. (A) Location of Cloșani Cave (CC, red, open star). The blue, filled star indicates Gümüşhane cave, NE Turkey (Jex et al., 2011). (B) Location of CC in the greater Carpathian area. Black stars: meteorological stations Targu Jiu (TJ, 203 m msl), Drobeta/Turnu Severin (DTS, 77 m msl) and GNIP station Râmnicu Vâlcea (RV, 237 m msl). The blue stars show the locations of regional studies mentioned in the text: the peat bog record from Sureanu (SU, Longman et al., 2017); the $\delta^{15}\text{N}$ guano record from Măgurici Cave (MC, Cleary et al., 2017); and the sediment record from Lake Ighiel (LI, Haliuc et al., 2017). (C) Seasonal precipitation distribution at TJ and DTS. Bars show the monthly precipitation amount and the mean value (TJ/DTS) of the two stations for 1961–1990. Potential evapotranspiration (PET, red line) and P-PET (green line) are shown for the mean value of both stations. (For interpretation of the colors in the figure(s), the reader is referred to the web version of this article.)

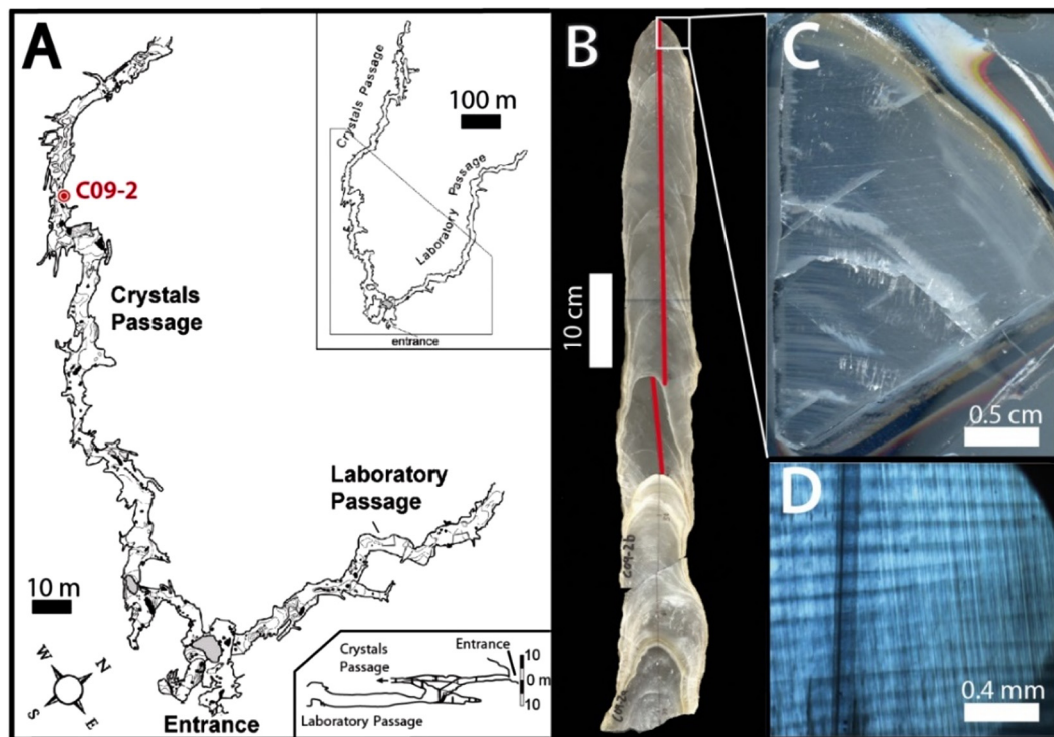


Fig. 2. (A) Map and cross section of Cloșani Cave indicating the location of stalagmite C09-2 prior to its removal in 2009. The cave map has been simplified after Diaconu (1990). (B) Scan of stalagmite C09-2, the red line indicates the main growth axis. This study focuses on the upper 46 cm of the sample. (C) Example of a slab used for LA-ICPMS measurements, showing macroscopically visible lamination, and (D) example of the lamination of C09-2 visible under the laser microscope.

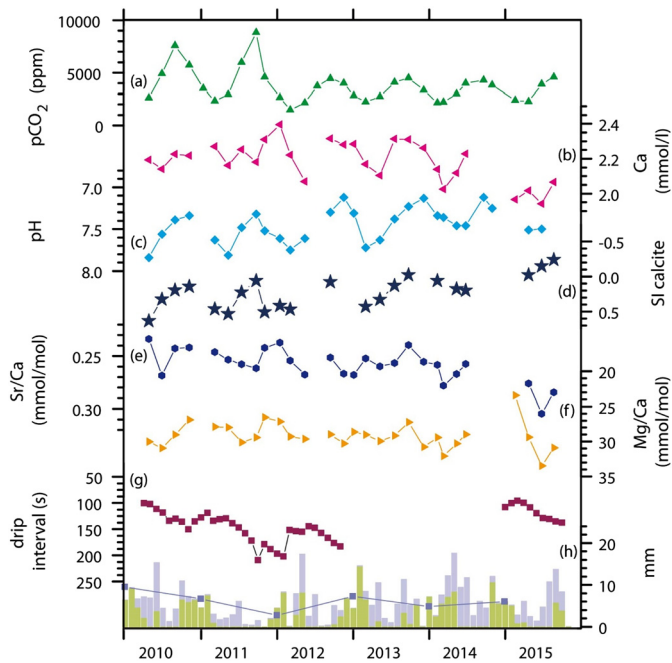


Fig. 3. Cave air and drip water in Cloşani Cave for drip site CC2 for the years 2010–2015. Values of $p\text{CO}_2$ (a), SI ((d), axis inverted) and pH ((c), axis inverted) show a pronounced seasonal signal, which is reflected in the Ca content (b) and also weakly visible in drip water Sr/Ca ((e), axis inverted) and Mg/Ca ((f), axis inverted). Purple squares (g) show monthly mean drip interval. Light blue bars (panel h) indicate monthly precipitation, green bars estimated infiltration (P–PET) and dark blue squares the mean values of the autumn/winter months (October to March) at Cloşani Cave, respectively.

dence intervals being valid also in the presence of autocorrelation.

3. Results and discussion

3.1. Monitoring

The seasonal precipitation cycle shows two maxima (Fig. 1C), one in early summer, mainly caused by North Atlantic cyclones, and a second peak in late autumn to early winter (October to December) generated by cyclones from the Mediterranean Basin (Micu et al., 2015). At both meteorological stations, each maximum accounts for approximately 30% of total annual precipitation (1920–1970), respectively. Estimation of potential evapotranspiration (PET, Fig. 1, Fig. 3h) shows that during summer, less than 25% of the precipitation is potentially available for infiltration, whereas during the cold season (October to March), 75 to 100% of the meteoric precipitation is available as recharge (supplementary text S1). At the altitude of the cave, snow fall accounts for about 7% of total annual precipitation amount and snow melt in spring occurs usually before end of March (Micu et al., 2015). Therefore, precipitation between October and March accounts for the major total annual infiltration.

Cave temperature shows a mean of 11.4°C with inter-annual variations of $\pm 0.5^\circ\text{C}$ and relative humidity being mostly close to 100%. Cave air $p\text{CO}_2$ exhibits a strong seasonal variability, with maximum values of up to 8800 ppmV of cave air in late summer and minimum values in winter and spring (about 2000 ppmV) following the seasonal temperature cycle at the surface (Fig. 3a). The pH of the drip water (Fig. 3c), Ca^{2+} concentration (Fig. 3b) and the calculated saturation indices (SI; Fig. 3d) follow the seasonal cave air CO_2 pattern suggesting that calcite precipitation is strongly favored in winter, and suppressed in summer months. This is confirmed by forward modeling using I-STAL (supplemental text S2)

as well as glass plates placed below drip sites, showing a noticeable amount of calcite precipitated during the cold season. Drip intervals are generally long with multiannual variations as well as a superimposed seasonal pattern following precipitation/infiltration amount with largest values of up to 200 s per drop during late summer and minima in early spring (about 100 s per drop, Fig. 3g). The variability of the $\delta^{18}\text{O}$ values in rain fall (GNIP station RV), drip water, recent and speleothem calcite is discussed in supplementary text S3.

3.2. Trace element variability

Initial drip water Mg/Ca, Sr/Ca (and Ba/Ca) ratios co-vary and show small amplitudes (Fig. 3e and f). The cross-plots (Fig. S2) of the logarithmic trace element to calcium ratios following the approach of Sinclair et al. (2012) show that the values in the drip water fit with the theoretically expected slopes of prior calcite precipitation (PCP) and/or incongruent calcite dissolution (ICD). In speleothem calcite, Sr/Ca and Ba/Ca ratios show also a strong coupling ($r_{\text{Sr/Ba}} = 0.96$, statistics of all given correlation coefficients summarized in Table S3), whereas in contrast to the drip water, Mg/Ca ratios are negatively correlated in speleothem calcite with Sr/Ca and Ba/Ca ($r_{\text{Mg/Sr}} = -0.45$ and $r_{\text{Mg/Ba}} = -0.46$).

Both Sr/Ca and Ba/Ca show pronounced alternating minima and maxima throughout most of the record, presumably on the seasonal scale (Fig. 4A). We argue, that the strong seasonal differences in calcite precipitation rates observed at the drip site lead to the strong seasonal cycles in Sr/Ca and Ba/Ca (Treble et al., 2003). Strong sub-annual growth rate variations over at least one order of magnitude, as forward modeled for drip site CC2 with I-STAL (supplemental text S2), exert a strong influence on the Sr (and Ba) incorporation into the calcite due to the dependency of the partitioning coefficients D_{Sr} and D_{Ba} on calcite precipitation rate (Fairchild and Treble, 2009; Huang and Fairchild, 2001). Inverse modeling of speleothem element/Ca ratios with I-STAL (Stoll et al., 2012) also confirms the dominant control of this process on Sr/Ca and Ba/Ca (supplementary text S2). In contrast, Mg/Ca in speleothem calcite is independent of growth rate, and the temperature dependency of D_{Mg} (Huang and Fairchild, 2001) can be regarded as negligible on the seasonal scale since the temperature in the cave is very constant. This relationship explains the decoupling of Mg/Ca ratios from Sr/Ca and Ba/Ca in the stalagmite in contrast to the drip water, where those are co-varying. Hence, the observed Sr/Ca (and Ba/Ca) cycles in C09-2 are interpreted to represent annual laminae, which can be counted to establish a precise age control (section 3.3) and, additionally, the laminae widths can be used as an indicator of mean annual growth rate.

The seasonal variability of the speleothem element/Ca ratios is superimposed on a generally stable signal, with variations on multi-annual to decadal scale (Fig. 4B). In order to assess potential drivers of this long-term trace element variability, I-STAL was again used as an inverse model (supplementary text S4). The model simulates multi-annual Mg/Ca, Sr/Ca (and Ba/Ca) variations in the speleothem with similar values to modern conditions of both drip interval and initial Ca content variability. Modeled drip intervals vary between 100 and 400 s, and initial Ca between 80 and 130 ppm (about 2–3 mmol/l). Thus, we interpret multi-annual Mg/Ca to be related with water–rock interaction processes determining the initial Ca content of the drip water, such as prior calcite precipitation (PCP) or incongruent calcite dissolution (ICD) (Fairchild and Treble, 2009; Sinclair et al., 2012).

A number of studies report an enrichment of Mg/Ca in drip waters and speleothem calcite during periods of low flow, e.g., Cruz et al. (2007), Johnson et al. (2006), McDonald et al. (2004), Treble et al. (2003). In addition, drip rate variability may influence the amount of deposited calcite (i.e. speleothem growth rate)

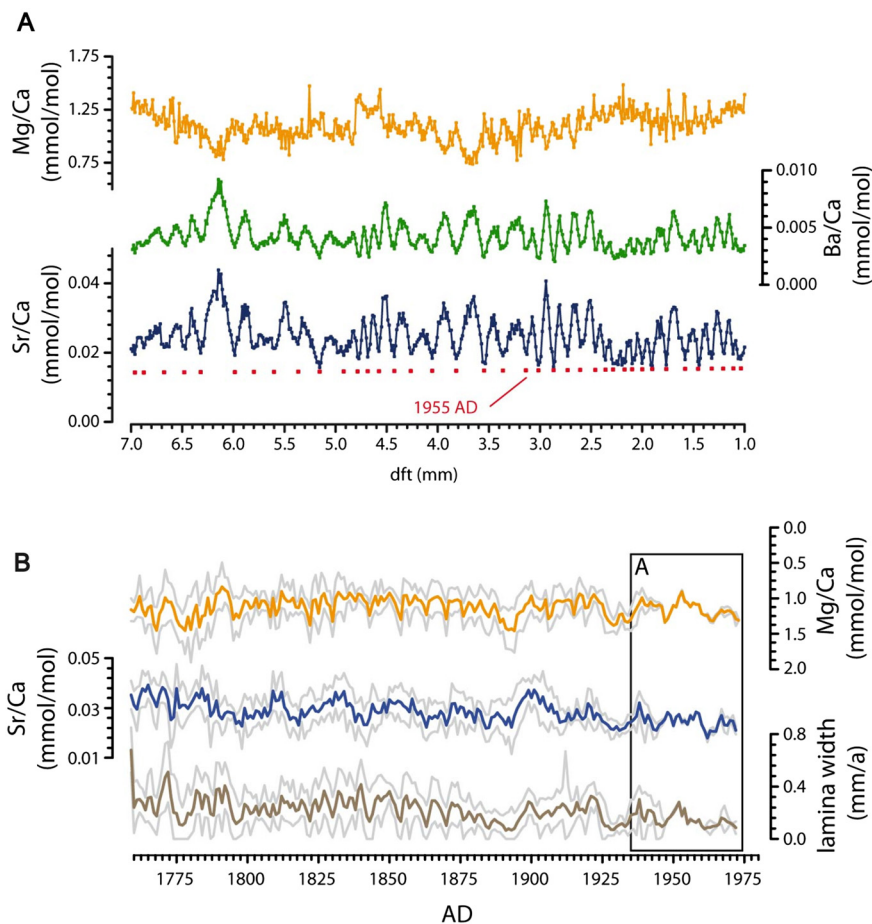


Fig. 4. (A) Raw Sr/Ca, Ba/Ca and Mg/Ca ratios in the top segment (7 to 1 mm dft) of stalagmite C09-2. Red points show minima allocated to the summer season. The reference point (AD 1955) is indicated at 3.2 mm dft. (B) Uppermost section of C09-2, based on a lamina-counted age model (AD 1759 to 1973). Mg/Ca (axis inverted), Sr/Ca ratios and lamina width are shown as annual means with the grey lines indicating the 95% confidence bands due to the variance of the lamina counting (section 3.3).

and, subsequently, its elemental composition (Casteel and Banner, 2015; Johnson et al., 2006; Kaufmann and Dreybrodt, 2004). Moreover, with increasing drip intervals, the degree of PCP increases thereby further lowering the saturation state of the drip water and increasing drip water elemental ratios (McDonald et al., 2004; Stoll et al., 2012). Sinclair et al. (2012) propose additional potential scenarios such as Mg input from dolomite dissolution or calcite recrystallization. However, these processes are not necessarily related to recharge, but may represent a second-order effect amplifying the enrichment of Mg during relatively dry conditions (Stoll et al., 2012). Sr/Ca (and Ba/Ca) ratios are also linked with these mechanisms, however, the growth rate effect on the partitioning coefficients due to seasonal cave air CO₂ variations seems to superimpose the variation in the initial drip water composition. Therefore, Sr/Ca (and Ba/Ca) ratios are used as indicators of annual lamination. From long lasting high Sr/Ca ratios on an annual scale we can attribute that the measured Mg/Ca is mainly a winter signal derived from water mainly infiltrating in the winter season (compare sec. 3.1 and 3.2). Hence, Mg/Ca ratios show the potential to provide information about past cool season hydroclimate variability.

3.3. Chronology

The observed seasonal variability of speleothem Sr/Ca was used to manually count chemical lamina to establish a precise age model and lamina width (i.e. the distance between two consecutive Sr/Ca minima) is used as indicator for mean annual growth rate (gr). Since the chemical lamina are not continuously devel-

oped, lamina counting was not possible beyond 47 mm dft, where the growth rate strongly decreases. In addition, the uppermost 1 mm is missing in the trace element record because it was lost during sample preparation. Between 1 and 47 mm dft, the width of annual lamina varies between 50 and 600 μm with a mean value of 210 μm .

¹⁴C measurements reveal a strong increase above 4 mm dft (Table S2 and Fig. S9). This increase in ¹⁴C activity is interpreted as the start of the mid-20th century atmospheric bomb peak recorded by the stalagmite. All published radiocarbon bomb peaks in speleothems, whose age models are based on laminar counting show that the response of speleothem ¹⁴C activity to the increase in atmospheric radiocarbon activity occurred nearly simultaneously (Fohlmeister et al., 2011; Hua et al., 2017). Therefore, we established the timing by identifying the last sample corresponding to the radiocarbon plateau of the early 20th century (sample “I” in Fig. S9) within ± 2 yr uncertainty of the start of the ¹⁴C increase in the stalagmite. This sets the reference point to the year AD 1955 at 3.2 mm dft (Fig. 4A). Counting of chemical lamina was repeated ten times by different investigators. Each series was anchored to the reference point of the year AD 1955. The distribution of the resulting chronologies allows to assess the uncertainty of lamina counting as standard deviations (sd) of the ensemble and the calculation of the mean age model (Fig. 5A). For the upper 47 mm dft, the sd of all chronologies is small (216 ± 3 counted chemical lamina). For the 20th century, the uncertainty of the lamina counting is only about ± 1 yr. Hence, taking into account the uncertainty of allocating the start of the ¹⁴C increase in the stalagmite (± 2 yr), the total uncertainties of this part amount to ± 3 yr.

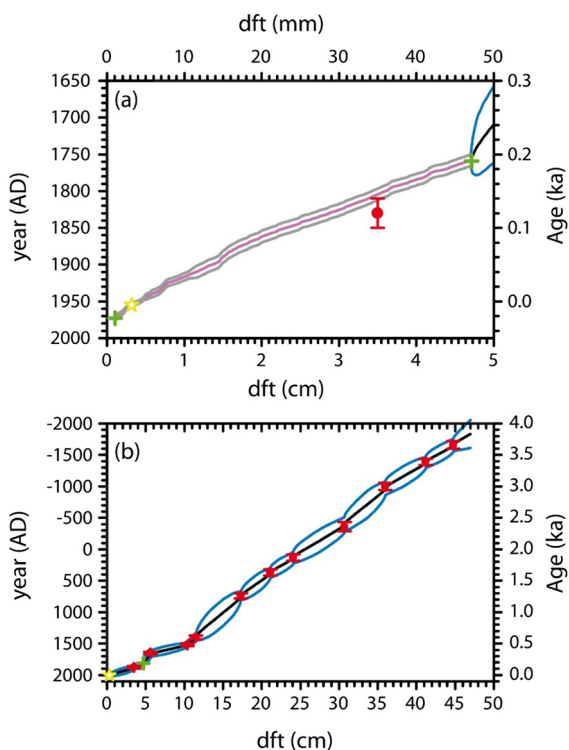


Fig. 5. Age-depth model of C09-2. Yellow star: position of the reference point (3.2 mm, AD 1955); green crosses: start (AD 1973) and end points (AD 1759) of the lamina counting; red points: ²³⁰Th/U ages. (A) Age models for the top 50 mm. Purple: age model obtained from lamina counting (grey: 2σ error including the ±2 yr uncertainty of the radiocarbon dating); black: age model using Bchron (Haslett and Parnell, 2008) (light blue: 2σ error). (B) Age-depth model and 2σ error obtained with Bchron.

In addition, eleven ²³⁰Th/U ages were determined in the upper 46 cm of the speleothem, which formed during the last 3.6 ka (Fig. 5B and Table S1). The ²³⁸U content of the stalagmite is generally low (on average 40–50 ng/g), and ²³²Th is below 50 pg/g in most samples. Relative errors of the ages range from 1.5 to 3% for the ages older than 600 yr. Due to the very low ²³⁰Th content (in the order of 5–10 fg/g), the age uncertainties of the two youngest samples are >5%.

The final age model (Fig. 5B) is divided into two parts. In the upper 47 mm, the combination of lamina counting and radiocarbon dating provides a precise age model (uncertainty ±3 yr) for the period from AD 1759 to 1973, which is in agreement within error with the uppermost ²³⁰Th/U-age (AD 1832 ± 29 at 35 mm dft) (Fig. 5A). Below, the age model is constructed based on the ²³⁰Th/U-ages using the R package ‘Bchron’ (Haslett and Parnell, 2008).

3.4. Instrumental calibration

The overlap of the stalagmite time series and the instrumental records of precipitation (1918–1973, $n = 55$) and temperature (1901 to 1973, $n = 69$) is used to explore potential links between climate parameters and the speleothem proxies (section 3.2). The proxy data seems independent of the instrumental temperature record. In contrast, a significant inverse correlation was found between speleothem Mg/Ca ratio and annual precipitation amount (July to June, $r_{Mg/P} = -0.42$, confidence intervals given in Table S4) as well as between Mg/Ca and autumn/winter precipitation (in the following labeled P_w) including the months of main infiltration October to March ($r_{Mg/P_w} = -0.42$) (Fig. 6). Both relationships are now further analyzed. To account for mixing of the infiltrating water of the previous years in the karst aquifer, the precip-

itation time series were smoothed with a 5-yr linearly weighted running mean using the weights $w_i = (1/2, 1/4, 1/8, 1/16, 1/16; \sum w_i = 1)$. This filter considers a stronger influence of more recent years in comparison to previous years (see e.g., Jex et al., 2011). This strategy is also motivated by the significantly increasing correlation of Mg/Ca to the 5-yr linearly weighted running mean $P_{w,rm}$ of autumn/winter precipitation to $r_{Mg/P_{w,rm}} = -0.58$ (Fig. 7A). The relation to annual precipitation also moderately increases to $r_{Mg/P,rm} = -0.48$. De-trending further improves the correlation to $r_{Mg/P_{w,rm}} = -0.61$ (Fig. 7B). Lamina widths (i.e. mean annual growth rates) show a positive trend of increased carbonate deposition with increased winter precipitation ($r_{gr/P_{w,rm}} = 0.37$), while a link to annual precipitation is statistically insignificant (Fig. 6). Consequently, for the period from AD 1759 to 1973 (Fig. 4B), annual lamina widths are negatively correlated to the annual mean Mg/Ca ratios ($r_{gr/Mg} = -0.67$), supporting the tight link of the two parameters. An alternative mixing model, which uses a mixture of fracture and storage flow (as proposed by Baker and Bradley (2010), Baker et al. (2007) and references therein), did not significantly improve the correlation of speleothem proxies and instrumental data, but suggests a simple reservoir with an overflow feeding stalagmite C09-2 (supplementary text S5).

The comparison with instrumental data indicates, that low growth rates and high Mg/Ca ratios of C09-2 occur during periods of relatively dry autumn/winter seasons. This confirms the previous interpretation of Mg/Ca variability as a proxy for complementary effects of water–rock interactions and varying drip interval (section 3.2) driven by changes in meteoric precipitation. The stronger connection to cool season precipitation can be explained by the fact that (1) most of the summer season precipitation is lost by evapotranspiration and that the karst reservoir is thus mainly fed by autumn and winter precipitation and (2) the strong seasonal bias of calcite precipitation rates (section 3.1). Mixing processes in the karst system act as a low-pass filter, explaining the highest correlation between Mg/Ca and cold season precipitation for the linearly weighted running mean of the precipitation time series over the previous 5 yr.

The robustness and significance of the marked anti-correlation between Mg/Ca and autumn/winter precipitation is further tested with respect to the uncertainties of the age model. For the calibration period between AD 1919 and 1973, the uncertainty of the lamina counting and the allocation of the reference years adds up to a total error of ±3 yr (section 3.3). We therefore incorporated the age uncertainties in the proxy signal using ensembles of age models, similar to the approach of Dee et al. (2015). A Monte Carlo (MC) routine was implemented, which randomly chooses one of the lamina counted age models A_n ($n = 10$) and the shift of the age scale between −3 and +3 yr. Subsequently, the corresponding correlation coefficient $r_{Mg/P_{w,i}}$ for the shifted time series $Mg/Ca_{shifted}$ was calculated. This routine simulates 1000 cross-correlations $r_{Mg/P_{w,i}}$ and calculates the mean of all $r_{Mg/P_{w,i}}$. This routine was repeated 1000 times (i.e. 1000×1000 simulations of $r_{Mg/P_{w,j}}$ in total) to calculate an overall mean correlation coefficient r_{Mg/P_w} and a corresponding standard deviation. The calculation of the means of the simulated correlation coefficients is based on Fisher’s Z transform. The produced MC ensembles of shifted element/Ca time series were also used to calculate the uncertainty bands of element/Ca due to age uncertainties.

Note that the probabilities of the directions of the shift are not equal. Shifting the bomb peak reference point by more than 2 yr towards younger ages is not possible because this would imply that the radiocarbon anomaly in the speleothem occurred prior the atmospheric signal. In contrast, it is conceivable (even if not likely, compare section 3.3) that the start of the ¹⁴C increase in the stalagmite might have been delayed by more than 3 yr. We emphasize this relationship by using the applied non-symmetric probability

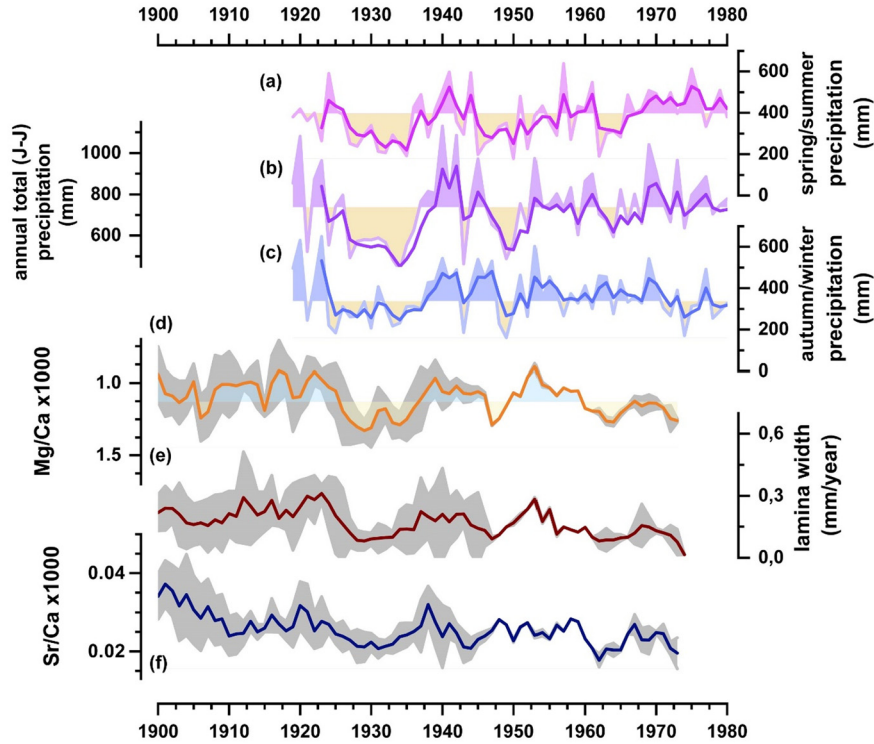


Fig. 6. Instrumental and proxy data 1900–1980. Upper panels: precipitation data: (a) spring/summer (AMJJAS), (b) annual total (June–July) and (c) autumn/winter (ONDJFM) precipitation; colored shadings of the instrumental time series indicate positive (negative) anomalies from mean values of the period 1961–1990, and thick lines the linearly weighted 5-yr running mean, respectively); lower panels: speleothem data (d) annual mean speleothem Mg/Ca (axis inverted), (e) annual mean lamina width and (f) annual mean speleothem Sr/Ca. Grey shadings indicate the 2σ -uncertainty due to lamina counting (section 3.4).

distribution of the possible shifts of the reference point (Fig. S10). The calculated overall mean value is $r_{Mg/Pw} = -0.46 \pm 0.14$ (standard deviation of 1000×1000 runs), which is still significant at a p -value of 0.1 (corrected for autocorrelation). The distribution of the r_{Mg/P_i} reaches maximum values of -0.60 and a mode of -0.53 , confirming the initial value of $r_{Mg/Pw,rm} = -0.58$ (Fig. S11).

Based on the robust, original correlation of $r_{Mg/Pw,rm} = -0.58$ for the calibration period (1919–1973), a quantitative estimate of past autumn/winter precipitation can be predicted, assuming that the correlation is valid for past conditions. The reconstruction is performed by fitting a linear regression model $P_{rec} = a \times Mg/Ca + c$ to the 5-yr linearly weighted running mean to predict precipitation from the Mg/Ca ratios in the speleothem. The resulting regression equation is (Fig. 7C):

$$P_{rec} = (-62 \pm 12) \times Mg/Ca + (130 \pm 14) \quad (1)$$

The uncertainties $\Delta(P_{rec})$ of the reconstructed estimates P_{rec} are based on the calculated prediction intervals of the regression $\Delta(P_{rec})_{pred}$ (Fig. 7C). However, the uncertainty of the age control of the Mg/Ca ratio also has to be accounted for. Therefore, the ensemble-based age uncertainty of Mg/Ca is taken into account:

$$\begin{aligned} \Delta(P_{rec})_{age} &= \partial P_{rec} / \partial Mg/Ca \times \Delta(Mg/Ca) \\ &= (62 \pm 12) \times \Delta(Mg/Ca) \end{aligned} \quad (2)$$

These uncertainties are then added to the prediction intervals from the regression analysis:

$$\Delta(P_{rec}) = \Delta(P_{rec})_{pred} + \Delta(P_{rec})_{age} \quad (3)$$

Fig. 7D shows that these uncertainties do not substantially increase the error band for the common period. However, they become

significant for the older parts with larger age uncertainties. The reconstructed precipitation amount, P_{rec} , explains 34% of the total variance of $P_{w,rm}$ ($r^2 = 0.34$). The original values of P_w and $P_{w,rm}$ are well within the estimated uncertainty bands (Fig. 7D).

The validity of the autumn/winter precipitation reconstruction was further assessed by applying a split calibration/verification approach to the instrumental and proxy data (Fritts, 1976). For the split approach, a random set of entries of the precipitation time series is omitted. This procedure is repeated $n = 30$ times. A separate regression model is then derived for each of the n new time series in which the precipitation observations and corresponding Mg/Ca ratios for the chosen years are omitted. The five years preceding every omitted year are also omitted in order to remove all information that is used to derive the linearly weighted running mean of the precipitation time series. This results in n independently derived estimates of winter precipitation that constitute a validation series. The validation series is then compared to the instrumental precipitation time series. A significant correlation was found between the precipitation estimates and the instrumental time series P_w ($r = 0.43$, $p < 0.05$). The standard deviation of the precipitation estimates is 7 mm.

3.5. Potential of the statistical and mechanistic models

Prior application of the transfer function (eq. (1)) to the Mg/Ca data of the older stalagmite sections, the influence of potential second order effects on the reconstruction have to be assessed. Since the Mg/Ca record is characterized by a general stability, a long-term persistence of the linear relationship of Mg/Ca in the speleothem to hydrological forcing can be assumed. This is illustrated by the similarity in the mean values and variances of the time series between the calibration period AD 1919–1973 ($1.13 \pm$

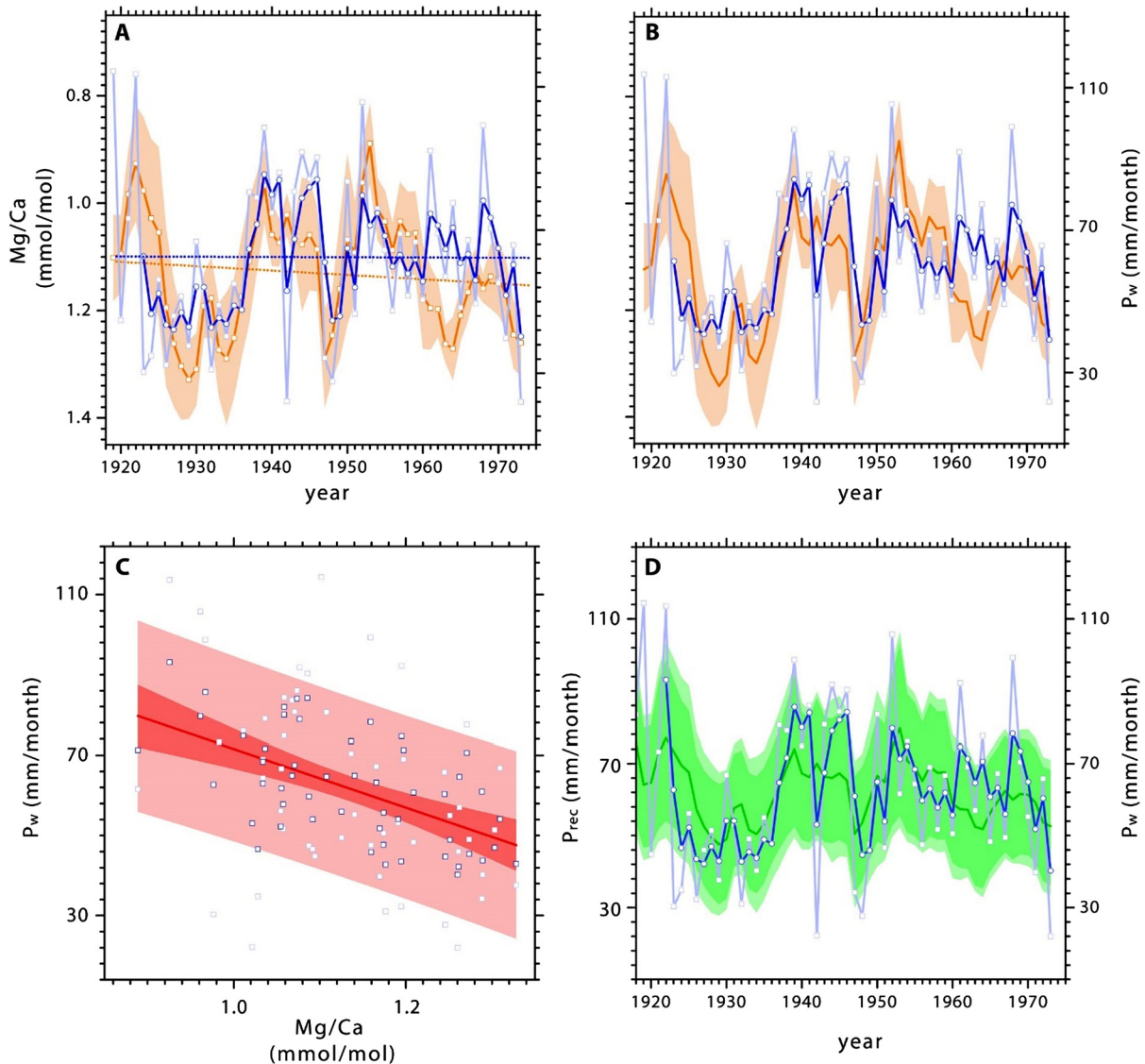


Fig. 7. Upper diagrams (A): Time series of Mg/Ca (orange) in speleothem C09-2, autumn/winter precipitation P_w (light blue) and the 5y linearly weighted running mean (RM) $P_{w,rm}$ (dark blue). Orange shaded bands indicate the ensemble-based uncertainty of Mg/Ca due to the error of the age control (see text for details). Dotted lines indicate the trend lines of the time series. (B): Detrended time series (linear trends indicated in panel (A)) of Mg/Ca, P_w and $P_{w,rm}$. Bottom panels: Results of regression analysis. (C) Regression model (red) applied to winter precipitation (mm) versus Mg/Ca ratio (mmol/mol). Light open symbols indicate ONDJFM precipitation values between 1919 and 1973, whereas dark open symbols show the 5y linearly weighted RM values. The shaded bands are 95% confidence (dark red) and 95% prediction (light red) bands. (D) Reconstructed precipitation time series P_{rec} (green) with prediction intervals (dark green shaded band) and final uncertainty bands including the error from the age control (light green shaded bands). Other lines indicate P_w (light blue) and $P_{w,rm}$ (dark blue).

0.11 mmol/mol) and the reconstruction period AD 1759–1918 (1.08 ± 0.13 mmol/mol).

However, a few short intervals in the C09-2 record suggest a short-term non-linear behavior of the system, indicated by very low growth rates, low Sr/Ca and very high Mg/Ca values. This comprises several short intervals of approximately 1 mm length or less (highlighted by the yellow bars in Fig. 8), such as the two most prominent periods around AD 1610 and between AD 1676 and 1716. Potential reasons for the observed phenomenon could be (1) a severe decline of water availability or (2) other scenarios not necessarily related to precipitation amount, like for example, non-linear processes during the residence time of water in the karst such as calcite recrystallization or Mg input from dolomite dissolution as well as very long drip intervals during periods of extremely low flow. The modern period at the top of the stalagmite can be most likely attributed to the first scenario, since Romania experienced a significant warming trend after the 1970s along with a very dry phase during the 1980s in the southern Carpathians (Micu

et al., 2015). This situation, however, cannot be clearly transferred to the other sections.

Extraordinary cold winter conditions with prolonged snow cover might be a conceivable, additional potential climatologic scenario. When the soil is permanently frozen, infiltration is not possible which may lead to higher Mg/Ca ratios in the speleothem even though the actual precipitation amount was high. In this case, the linear regression model would underestimate the actual value. In general, this is not a likely scenario at the site due to the southward exposure of the overlying hill slope, the buffering effect of the thick host rock overburden and the moderate elevation (<500 mmsl). At such low elevations snow fall accounts for only about 7% of total annual precipitation (Micu et al., 2015) and moreover, snow cover acts as an effective insulation layer, keeping soil temperatures above the freezing point despite air temperatures below 0°C (Vasile et al., 2014). Thus, snow cover should not largely influence infiltration. As a precaution, these problematic sections were however excluded from the Mg/Ca record prior to the ap-

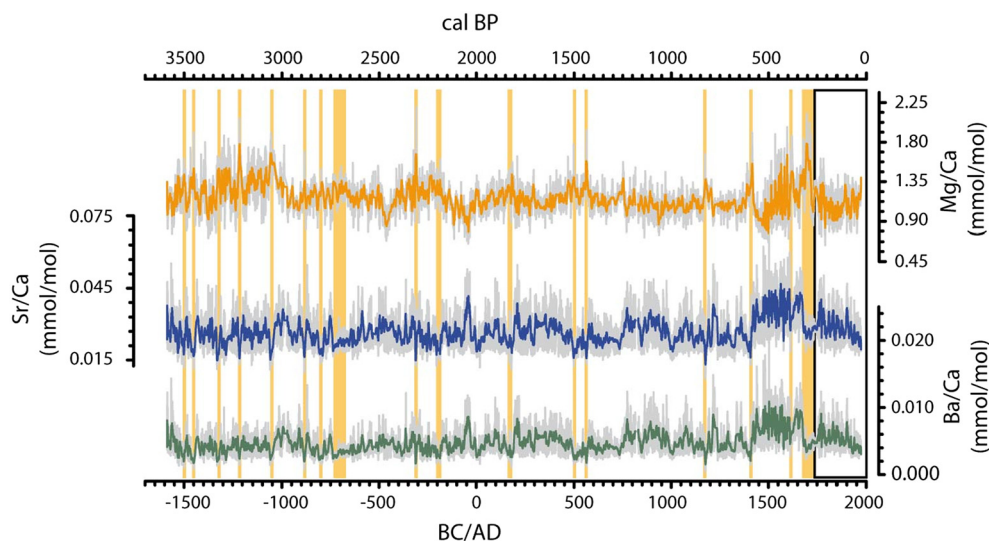


Fig. 8. Complete C09-2 trace element record. Element/Ca ratios are presented in temporal resolutions of 1 yr (light grey lines) and 5 yr (colored lines). Short-term sections with poorly developed lamination, low Sr/Ca and high Mg/Ca, indicating slow speleothem growth, are highlighted by orange vertical bars. The black rectangle indicates the section shown in Fig. 4B.

plication of the transfer function to prevent erroneous inferences from our reconstruction.

The linear regression model explains about 34% of the variance of total autumn/winter precipitation. The relatively high remaining unexplained variance of proxy calibrations can be partially ascribed to higher frequency variations, which are eliminated when using regression approaches (Esper et al., 2005). In this case study, these could e.g. stem from the pronounced sub-annual variability which is also in parts visible in the Mg/Ca ratios (Fig. 4), as well as potentially non-linear effects during periods of extremely low infiltration as described in the previous paragraph. Another factor is the uncertainty of the instrumental precipitation data. The correlation of the precipitation time series between the stations TJ and DTS is $r = 0.87$ (supplemental text S2), illustrating that about 20% of the variance may be subject to local incongruities of precipitation patterns. In addition, the influence of warm season precipitation may be under-estimated during cool and/or wet summers with low PET, leading to small variations of the assumed main infiltration period between October and March.

Finally, the observed correlation in this study is in good agreement with other drip water and/or speleothem proxy calibration studies, which also report only moderate values of r^2 between 20% and 50% (e.g., Baker et al., 2007; Cai et al., 2010; Jex et al., 2011; Moquet et al., 2016; Tan et al., 2013), illustrating that a high unexplained variability is inherent to most systems used for proxy calibration studies. We conclude that the regression approach in combination with the mechanistic model is sufficiently robust to allow further application and hence the transfer function (eq. (1)) is used to produce estimates of the amount of winter precipitation (mm/month) from 1700 BC–AD 1973.

3.6. Late Holocene climate variability in SW Romania

Model studies report a relationship of winter precipitation in the Carpathian–Balkan realm with dominant North Atlantic atmospheric circulation patterns during the 20th century, with positive precipitation anomalies in Romania during weaker phases of the North Atlantic Oscillation (NAO) and vice versa (Bojariu and Paliu, 2001). Although some paleo-hydrological reconstructions suggest that this connection persisted in the past (Cleary et al., 2017; Longman et al., 2017), many studies found incongruities in temporal correlation and interferences with the Mediterranean circulation (e.g., Constantin et al., 2007; Onac et al., 2002; Roberts et

al., 2012). This picture is confirmed when comparing the C09-2 precipitation estimates during the late Holocene since 3.6 kaBP (Fig. 9) with reconstructions of NAO strength (Olsen et al., 2012; Trouet et al., 2009) and other paleo-hydrological reconstructions from the Romanian Carpathians (Haliuc et al., 2017; Longman et al., 2017).

Between 3600 and 2500 cal. BP, a generally dry climate in SW Romania (Fig. 9b) is in accordance with a long phase of slightly positive indexes of the NAO (Fig. 9a), but in contrast to increased detrital sedimentation in Lake Igheal north of the Carpathians (Fig. 9d). In this phase, Haliuc et al. (2017) report a strong NW–SE hydro-climatic gradient with contrasting precipitation signatures in Central Europe and north of the Carpathians compared to the Balkan region. This pattern suggests that the influence of North Atlantic circulation changed from a positive to a negative correlation when crossing the Carpathian mountain chain from northwest to southeast. Interestingly, during the late Bronze Age, around 1300–1000 BC, a very dry interval is recorded in different records south (this study; Constantin et al., 2007) and north of the Carpathians (Haliuc et al., 2017; Onac et al., 2002), indicating that the edge of North Atlantic forcing drew back further west.

The Roman Warm Period (RWP, 250 BC–AD 400) was characterized by generally humid conditions in SW Romania in the first half and a drier period from 0 to AD 200 (Fig. 9b). Concurrently, the NAO indexes tend from negative to positive values. Similarly, the beginning of the Medieval Climate Anomaly (MCA) between ca. AD 900 and 1200 was more humid than average in Cloșani, whereas conditions became drier and similar to modern conditions during the second half of the MCA until 1430 (Fig. 9b). This drying trend during the MCA was identified across the Romanian Carpathians in Sureanu peat bog (Fig. 9c), Lake Igheal (Fig. 9d) and Musca Cave, SW Romania (Onac et al., 2014). A persistent positive NAO mode during the late MCA may have been a reason for this drying trend in Romania (Olsen et al., 2012; Trouet et al., 2009), even though the influence is not as obvious as during other parts of the record (Fig. 9).

The onset of the Little Ice Age (LIA) until AD 1600 documents similar to modern conditions followed by a drying trend until 1675 (Fig. 9b), even though no direct connection to NAO variability is visible. We point out, that extremely low growth rates and very high Mg/Ca ratios in C09-2 indicate, that this drying was at its maximum between 1675 and 1715. A dry LIA in Romania is also reported in Lake Igheal (Fig. 9d), a peat bog profile from the north-

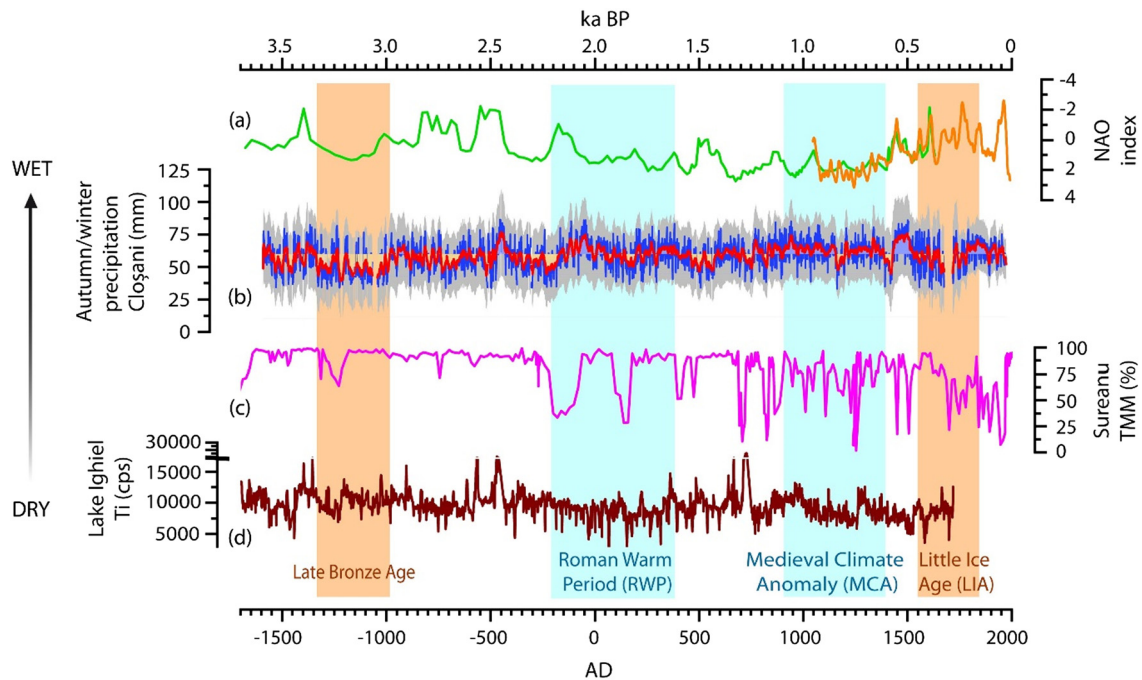


Fig. 9. Comparison of regional hydroclimate reconstructions with (a) strength of North Atlantic forcing, indicated by the NAO index reconstructions (axis inverted) from Olsen et al. (2012) (green line) and Trouet et al. (2009) (orange line). (b) Autumn/winter precipitation reconstruction from stalagmite C09-2, Cloșani (SW Romania). (c) Total Minerogenic Matter (TMM) from Sureanu peat, southern Carpathians (Longman et al., 2017), (d) Ti record from Lake Ighiel, northwest of the Carpathians (Haliuc et al., 2017). Orange bars indicate relatively dry and blue bars relatively humid climate anomalies in SW Romania as documented in other regional and European studies (see text for more detail).

ern Carpathians (Feurdean et al., 2015) and Nar lake in central Turkey (Roberts et al., 2012). The LIA is known as a pronounced cold phase in Europe with occasional very heavy snow events also in the Mediterranean area (Diodato et al., 2014). Longman et al. (2017) interpret the increased deposition of clastic material in Sureanu peat bog (elevation 1840 m asl) with events of snow avalanches. Hence, we hypothesize that during this interval, also at the low elevation of Cloșani infiltration may have decreased to a minimum due to very cold winters with enhanced snow-cover (section 3.5).

In summary, on the centennial to millennial timescales, the Cloșani precipitation estimates are in accordance with the presumed relation of regional precipitation with NAO variability, in particular over large parts of the 3100 yr between 1600 BC and AD 1500 (Fig. 9). However, this connection weakens e.g., from 850 to 500 BC, 200 to 50 BC and AD 490 to 620.

In the following, we will take advantage of the high temporal resolution of our record and further investigate the regional stationarity of the NAO–Pw relationship. In Fig. 10, the speleothem derived lamina widths and precipitation estimates are compared to the $\delta^{15}\text{N}$ guano record from Măgurici Cave (MC), NW Romania (Cleary et al., 2017) which is interpreted to reflect NAO related winter precipitation variability, and the speleothem $\delta^{18}\text{O}$ derived autumn/winter rainfall reconstruction from northern Turkey (Jex et al., 2011), which is mainly influenced by the EAWR. Indeed, over large parts the records seem to be related qualitatively, with the C09-2 reconstruction and the MC $\delta^{15}\text{N}$ record showing remarkable similarities on multi-decadal to centennial timescales, indicative of a common, regional precipitation pattern. The greater part of the 19th century and the period between AD 1900 and 1925 are both characterized by positive precipitation anomalies in NW and SW Romania and comparably humid conditions in NW Turkey. Relatively dry periods in both Romania and Turkey are recorded between AD 1765 and 1770, around AD 1800 and during the years AD 1926–1936. Similarly, the decline in growth rate during the AD 1970s in C09-2 occurred simultaneously to a strong decrease

in MC $\delta^{15}\text{N}$ corresponding to a strong reduction in precipitation. This particular shift may be associated with a change from negative to positive phase of both the NAO and the EAWR (Cleary et al., 2017). In contrast, no clear correlation of precipitation anomalies in Cloșani distinct NAO phases (Ortega et al., 2015) can be identified for other prominent intervals. Moreover, some dry spells, such as AD 1775–1785, around AD 1820 and AD 1885–1895, occurred only in SW and NW Romania, whereas during others (e.g., AD 1947–1949 or AD 1960–1966) precipitation anomalies appear to have declined only in the southern and eastern parts of the region, while the western part remained relatively humid (Fig. 10). This intermittently occurring decoupling along the NW–SE axis suggests that the common dominant influence of western circulation sporadically shifted across the Carpathian/Balkan region.

Our observation of periodically weakened influence of the NAO in the southern Carpathians was also previously made by Longman et al. (2017), who on the one hand found evidence for the sensitivity of the area with relatively small fluctuations in NAO intensity, with the timing of flooding events apparently correlating to periods of weakened NAO. On the other hand, Longman et al. (2017) noted a decreasing impact of the NAO on climate from Western Europe eastwards through Eurasia. This observation was also made by Haliuc et al. (2017), who report strong NW/SE hydrological gradients across central Europe and the Balkans periodically occurring during the late Holocene. Similarly, Roberts et al. (2012) concluded, that the late Holocene hydro-climatic pattern in the Mediterranean realm was determined by a combination of climate modes, such as the East Atlantic–Western Russia pattern (EAWR), and not solely by NAO forcing.

A number of modeling studies have shown this temporal and spatial interferences of the centers of action of dominant European low-frequency oscillations such as NAO or EAWR during the 20th century (Bojariu and Paliu, 2001; Comas-Bru and McDermott, 2014; Krichak et al., 2002, 2014). For instance, jointly acting positive (negative) phases of both the NAO and EAWR are associated with negative (positive) winter precipitation anomalies across the

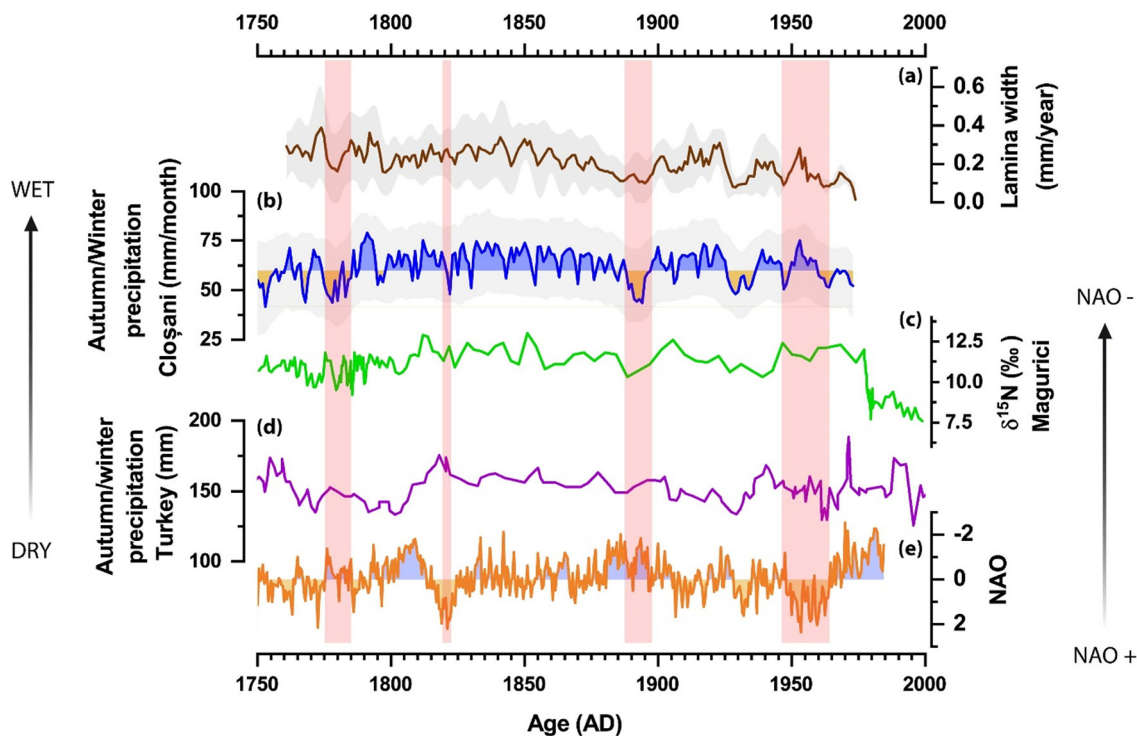


Fig. 10. Lamina widths (a) and reconstructed autumn/winter precipitation (b) based on the Mg/Ca ratio of stalagmite C09-2. Grey bands in (a) and (b) indicate the uncertainties of the reconstructed rainfall and growth rate. Blue (yellow) shading indicates wetter (drier) years than the mean values of the common period (AD 1919–1973); (c) $\delta^{15}\text{N}$ guano record from Măgurici Cave (MC), NW Romania (Cleary et al., 2017), reflecting NAO related winter precipitation; (d) autumn/winter rainfall reconstruction from NE Turkey by Jex et al. (2011); (e) NAO index reconstruction (axis inverse) from Ortega et al. (2015). Blue (orange) shadings indicate negative (positive) phases of the NAO presumably associated with wetter (drier) conditions in Romania. Vertical bars indicate phases of intermittently occurring decoupling of North Atlantic forcing from precipitation patterns along the NW–SE axis in the Carpathian/Balkan region (compare text in section 3.6).

Eastern Mediterranean (EM) including the Carpathian/Balkan realm (Ionita, 2014; Krichak et al., 2002). In contrast, during phases of opposite signs of both patterns, the eastern edge of dominant NAO influence moves back towards the western and northern Mediterranean (Krichak et al., 2002). Hence, we favor the interplay of NAO and EAWR forcing as a dominant scenario for the observed precipitation variability in the Carpathian–Balkan realm.

4. Conclusions

This study is one of the first demonstrating the potential of a speleothem Mg/Ca record for quantitative precipitation reconstruction. We show, that transferring a qualitative measure of coherence allows for a statistical meaningful, first order empirical reconstruction of precipitation. For this purpose, important prerequisites are a very high resolution of a laminated speleothem as well as a sufficient long calibration period.

Hence, despite the presence of dating uncertainties and other second-order effects, our method allows the reliable reconstruction of autumn/winter precipitation from speleothem Mg/Ca even though the applied regression model only explains roughly 34% of total precipitation variability. Therefore, our approach represents a valuable template for future studies intending quantitative climate reconstruction from speleothem proxies.

Our resulting high resolution autumn/winter precipitation reconstruction gives new insight on past hydroclimate in the Carpathian/Balkan realm and helps to understand its spatial and temporal variability. In accordance with previous studies, our record generally confirms the connectivity of autumn/winter precipitation to North Atlantic forcing on centennial to millennial timescales. However, our results also suggest a strong regional forcing of hydro-climate in the Romanian Carpathians in particular and a non-persistent relationship to the NAO especially on

(multi-) annual to decadal timescales. To disentangle possible influences e.g., from the EAWR, on precipitation patterns further regional paleo-hydrological reconstructions are desirable.

Acknowledgements

This project was funded by the German Science Foundation (DFG grants SCHO 1274/6-1 and SCHO/9-1) and the DFG Research Group 668 (DAPHNE) and also benefited from the support of MC-ICPMS infra-structure through grant DFG-INST 35_1143-1 FUGG. Cave monitoring was supported through the CAVEMONITOR Project (Grant 17SEE/2014) and CARPATHEMS Project (Grant PCE 197/2016) (both to SC). We also acknowledge the data providers in the ECA&D project (Klein Tank et al. (2002), data and metadata available at <http://www.ecad.eu>).

The anonymous reviewers are thanked for their helpful comments that improved the manuscript. We explicitly appreciate the support and commitment of the editor.

The authors are further grateful to René Eichstädter, Manuela Wimmer, Sylvia Riechelmann, Anne Marie Wefing, Hanna Rosentahl and Arno Hartmann for assistance in the laboratory and with data acquisition. Kira Rehfeld and Michael Deininger are thanked for helpful discussions.

Appendix A. Supplementary material

Supplementary material related to this article can be found online at <https://doi.org/10.1016/j.epsl.2018.07.027>.

References

- Baker, A., Asrat, A., Fairchild, I.J., Leng, M.J., Wynn, P.M., Bryant, C., Genty, D., Umer, M., 2007. Analysis of the climate signal contained within $\delta^{18}\text{O}$ and growth

- rate parameters in two Ethiopian stalagmites. *Geochim. Cosmochim. Acta* 71, 2975–2988.
- Baker, A., Bradley, C., 2010. Modern stalagmite $\delta^{18}\text{O}$: instrumental calibration and forward modelling. *Glob. Planet. Change* 71, 201–206.
- Bojariu, R., Paliu, D.-M., 2001. North Atlantic Oscillation projection on Romanian climate fluctuations in the cold season. In: *Detecting and Modelling Regional Climate Change*. Springer, pp. 345–356.
- Cai, B., Pumijumnong, N., Tan, M., Muangsong, C., Kong, X., Jiang, X., Nan, S., 2010. Effects of intraseasonal variation of summer monsoon rainfall on stable isotope and growth rate of a stalagmite from northwestern Thailand. *J. Geophys. Res., Atmos.* 115.
- Casteel, R.C., Banner, J.L., 2015. Temperature-driven seasonal calcite growth and drip water trace element variations in a well-ventilated Texas cave: implications for speleothem paleoclimate studies. *Chem. Geol.* 392, 43–58.
- Cleary, D.M., Wynn, J.G., Ionita, M., Forray, F.L., Onac, B.P., 2017. Evidence of long-term NAO influence on East-Central Europe winter precipitation from a guano-derived $\delta^{15}\text{N}$ record. *Sci. Rep.* 7, 14095.
- Comas-Bru, L., McDermott, F., 2014. Impacts of the EA and SCA patterns on the European twentieth century NAO-winter climate relationship. *Q. J. R. Meteorol. Soc.* 140, 354–363.
- Constantin, S., Bojar, A.-V., Lauritzen, S.-E., Lundberg, J., 2007. Holocene and Late Pleistocene climate in the sub-Mediterranean continental environment: a speleothem record from Poleva Cave (Southern Carpathians, Romania). *Palaeogeogr. Palaeoclimatol. Palaeoecol.* 243, 322–338.
- Constantin, S., Lauritzen, S.-E., 1999. Speleothem datings in SW Romania. Part 1: evidence for a continuous speleothem growth in Pestera Ciosani during oxygen isotope stages 5–3 and its paleoclimatic significance. *Theor. Appl. Karstol.* 11–12, 35–46.
- Cruz, F.W., Burns, S.J., Jercinovic, M., Karmann, I., Sharp, W.D., Vuille, M., 2007. Evidence of rainfall variations in Southern Brazil from trace element ratios (Mg/Ca and Sr/Ca) in a Late Pleistocene stalagmite. *Geochim. Cosmochim. Acta* 71, 2250–2263.
- Dee, S., Emile-Geay, J., Evans, M.N., Allam, A., Steig, E.J., Thompson, D.M., 2015. PRYSM: an open-source framework for PProX System Modeling, with applications to oxygen-isotope systems. *J. Adv. Model. Earth Syst.* 7, 1220–1247.
- Diaconu, G., 1990. Cloșani Cave. Mineralogic and Genetic Study of Carbonate and Clays. Inst. Speol. “E. Racoviță”, București.
- Diodato, N., Bellocchi, G., Bertolin, C., Camuffo, D., 2014. Climate variability analysis of winter temperatures in the central Mediterranean since 1500 AD. *Theor. Appl. Climatol.* 116, 203–210.
- Esper, J., Frank, D.C., Wilson, R.J., Briffa, K.R., 2005. Effect of scaling and regression on reconstructed temperature amplitude for the past millennium. *Geophys. Res. Lett.* 32.
- Fairchild, I.J., Treble, P.C., 2009. Trace elements in speleothems as recorders of environmental change. *Quat. Sci. Rev.* 28, 449–468.
- Feurdean, A., Galka, M., Kuske, E., Tantau, I., Lamentowicz, M., Florescu, G., Liakka, J., Hutchinson, S.M., Mulch, A., Hickler, T., 2015. Last millennium hydroclimate variability in Central–Eastern Europe (northern Carpathians, Romania). *Holocene* 25, 1179–1192.
- Fohlmeister, J., Kromer, B., Mangini, A., 2011. The influence of soil organic matter age spectrum on the reconstruction of atmospheric ^{14}C levels via stalagmites. *Radiocarbon* 53, 99–115.
- Fritts, H., 1976. *Tree Rings and Climate*. Academic, San Diego, Calif. 567 pp.
- Haliuc, A., Veres, D., Brauer, A., Hubay, K., Hutchinson, S.M., Begy, R., Braun, M., 2017. Palaeohydrological changes during the mid and late Holocene in the Carpathian area, central-eastern Europe. *Glob. Planet. Change* 152, 99–114.
- Haslett, J., Parnell, A., 2008. A simple monotone process with application to radiocarbon-dated depth chronologies. *J. R. Stat. Soc., Ser. C, Appl. Stat.* 57, 399–418.
- Hua, Q., Cook, D., Fohlmeister, J., Penny, D., Bishop, P., Buckman, S., 2017. Radiocarbon dating of a speleothem record of paleoclimate for Angkor, Cambodia. *Radiocarbon*, 1–18.
- Huang, Y., Fairchild, I.J., 2001. Partitioning of Sr^{2+} and Mg^{2+} into calcite under karst-analogue experimental conditions. *Geochim. Cosmochim. Acta* 65, 47–62.
- Ionita, M., 2014. The impact of the East Atlantic/Western Russia pattern on the hydroclimatology of Europe from mid-winter to late spring. *Climate* 2, 296–309.
- Jex, C.N., Baker, A., Eden, J.M., Eastwood, W.J., Fairchild, I.J., Leng, M.J., Thomas, L., Sloane, H.J., 2011. A 500 yr speleothem-derived reconstruction of late autumn–winter precipitation, northeast Turkey. *Quat. Res.* 75, 399–405.
- Johnson, K., Hu, C., Belshaw, N., Henderson, G., 2006. Seasonal trace-element and stable-isotope variations in a Chinese speleothem: the potential for high-resolution paleomonsoon reconstruction. *Earth Planet. Sci. Lett.* 244, 394–407.
- Kaufmann, G., Dreybrodt, W., 2004. Stalagmite growth and palaeo-climate: an inverse approach. *Earth Planet. Sci. Lett.* 224, 529–545.
- Klein Tank, A.M.G., et al., 2002. Daily dataset of 20th-century surface air temperature and precipitation series for the European climate assessment. *Int. J. Climatol.* 22, 1441–1453.
- Krichak, S., Kishcha, P., Alpert, P., 2002. Decadal trends of main Eurasian oscillations and the Eastern Mediterranean precipitation. *Theor. Appl. Climatol.* 72, 209–220.
- Krichak, S.O., Breitgand, J.S., Gualdi, S., Feldstein, S.B., 2014. Teleconnection–extreme precipitation relationships over the Mediterranean region. *Theor. Appl. Climatol.* 117, 679–692.
- Levanič, T., Popa, I., Poljanšek, S., Nechita, C., 2012. A 323-year long reconstruction of drought for SW Romania based on black pine (*Pinus nigra*) tree-ring widths. *Int. J. Biometeorol.* 57, 703–714.
- Longman, J., Ersek, V., Veres, D., Salzmann, U., 2017. Detrital events and hydroclimate variability in the Romanian Carpathians during the mid-to-late Holocene. *Quat. Sci. Rev.* 167, 78–95.
- McDonald, J., Drysdale, R., Hill, D., 2004. The 2002–2003 El Niño recorded in Australian cave drip waters: implications for reconstructing rainfall histories using stalagmites. *Geophys. Res. Lett.* 31.
- Micu, D.M., Dumitrescu, A., Cheval, S., Birsan, M.-V., 2015. *Climate of the Romanian Carpathians*. Springer.
- Moquet, J.S., Cruz, F.W., Novello, V.F., Strikis, N.M., Deininger, M., Karmann, I., Santos, R.V., Millo, C., Apaestegui, J., Guyot, J.L., Siffedine, A., Vuille, M., Cheng, H., Edwards, R.L., Santini, W., 2016. Calibration of speleothem $\delta^{18}\text{O}$ records against hydroclimate instrumental records in Central Brazil. *Glob. Planet. Change* 139, 151–164.
- Ólafsdóttir, K., Mudelsee, M., 2014. More accurate, calibrated bootstrap confidence intervals for estimating the correlation between two time series. *Math. Geosci.* 46, 411–427.
- Olsen, J., Anderson, N.J., Knudsen, M.F., 2012. Variability of the North Atlantic Oscillation over the past 5200 years. *Nat. Geosci.* 5, 808.
- Onac, B.P., Constantin, S., Lundberg, J., Lauritzen, S.-E., 2002. Isotopic climate record in a Holocene stalagmite from Ursilor Cave (Romania). *J. Quat. Sci.* 17, 319–327.
- Onac, B.P., Forray, F.L., Wynn, J.G., Giurgiu, A.M., 2014. Guano-derived $\delta^{13}\text{C}$ -based paleo-hydroclimate record from Gaura cu Musca Cave, SW Romania. *Environ. Earth Sci.* 71, 4061–4069.
- Ortega, P., Lehner, F., Swingedouw, D., Masson-Delmotte, V., Raible, C.C., Casado, M., Yiou, P., 2015. A model-tested North Atlantic Oscillation reconstruction for the past millennium. *Nature* 523, 71.
- Popa, I., Kern, Z., 2008. Long-term summer temperature reconstruction inferred from tree-ring records from the Eastern Carpathians. *Clim. Dyn.* 32, 1107–1117.
- Roberts, N., Moreno, A., Valero-Garcés, B.L., Corella, J.P., Jones, M., Alcock, S., Woodbridge, J., Morellón, M., Luterbacher, J., Xoplaki, E., et al., 2012. Palaeolimnological evidence for an east–west climate see-saw in the Mediterranean since AD 900. *Glob. Planet. Change* 84, 23–34.
- Sinclair, D.J., Banner, J.L., Taylor, F.W., Partin, J., Jenson, J., Mylroie, J., Goddard, E., Quinn, T., Jocspon, J., Miklavič, B., 2012. Magnesium and strontium systematics in tropical speleothems from the Western Pacific. *Chem. Geol.* 294, 1–17.
- Smith, C.L., Fairchild, I.J., Spötl, C., Frisia, S., Borsato, A., Moreton, S.G., Wynn, P.M., 2009. Chronology building using objective identification of annual signals in trace element profiles of stalagmites. *Quat. Geochronol.* 4, 11–21.
- Stoll, H.M., Müller, W., Prieto, M., 2012. I-STAL, a model for interpretation of Mg/Ca, Sr/Ca and Ba/Ca variations in speleothems and its forward and inverse application on seasonal to millennial scales. *Geochem. Geophys. Geosyst.* 13.
- Tan, L., Yi, L., Cai, Y., Shen, C.-C., Cheng, H., An, Z., 2013. Quantitative temperature reconstruction based on growth rate of annually-layered stalagmite: a case study from central China. *Quat. Sci. Rev.* 72, 137–145.
- Thornthwaite, C.W., 1948. An approach toward a rational classification of climate. *Geogr. Rev.* 38, 55–94.
- Treble, P., Shelley, J.M.G., Chappell, J., 2003. Comparison of high resolution sub-annual records of trace elements in a modern (1911–1992) speleothem with instrumental climate data from southwest Australia. *Earth Planet. Sci. Lett.* 216, 141–153.
- Trouet, V., Esper, J., Graham, N.E., Baker, A., Scourse, J.D., Frank, D.C., 2009. Persistent positive North Atlantic oscillation mode dominated the Medieval Climate Anomaly. *Science* 324, 78–80.
- Vasile, M., Vespremeanu-Stroe, A., Popescu, R., 2014. Air versus ground temperature data in the evaluation of frost weathering and ground freezing. Examples from the Romanian Carpathians. *Rev. Geomorfol.* 16.
- Zwiers, F.W., von Storch, H., 1995. Taking serial correlation into account in tests of the mean. *J. Climate* 8, 336–351.